Int. J. Heat Mass Transfer. Vol. 31, No. 6, pp. 1237–1245, 1988
Printed in Great Britain

0017–9310/88 $3.00 + 0.00

Heat transfer and pressure drop characteristics in a corrugated duct with rounded corners

YUTAKA ASAKO and HIROSHI NAKAMURA
Department of Mechanical Engineering, Tokyo Metropolitan University, Tokyo, Japan

and

MOHAMMAD FAGHRI
Department of Mechanical Engineering and Applied Mechanics, University of Rhode Island, Kingston, RI 02881, U.S.A.

(*Received* 20 *January* 1987 *and in final form* 30 *October* 1987)

Abstract—Heat transfer and pressure drop responses of a corrugated duct with rounded corners were determined numerically. The duct boundaries were approximated by a cosine function. Computations were carried out for a Prandtl number of 0.7, in the Reynolds number range from 100 to 1000, for three assigned corrugation angles, and for four values of aspect ratios. Rounding of the corners resulted in a decrease of friction factor and Nusselt number. Heat transfer performance of a duct with rounded corners was compared to a straight duct and to a duct with sharp corners under three different constraints: fixed pumping power, fixed pressure drop, and fixed mass flow. The heat transfer rates decreased or increased depending on the specific conditions.

INTRODUCTION

CORRUGATED ducts are often utilized in the design of compact heat exchangers because of their efficient heat exchange capability. Izumi *et al.* [1, 2] reported numerical solutions for laminar flow and heat transfer in a corrugated duct with two right-angle bends and investigated the effect of bending angle on the heat transfer and fluid flow characteristics. Amano [3, 4] also studied corrugated ducts with right-angle bends numerically for both laminar and turbulent flows and compared the results with the experimental work by Izumi *et al.* [5]. The numerical solutions for corrugated ducts with periodically fully developed flow and heat transfer were reported by Izumi *et al.* [6] and Amano [7]. Asako and Faghri [8] extended the latter problem for channels with an arbitrary bend angle by employing a coordinate transformation methodology [9].

With the exception of a recent paper by Sparrow and Hossfeld [10] who measured pressure drop and heat transfer rates for a periodically corrugated duct with rounded corners, there is no single investigation to study the effect of rounding of duct corners. This has motivated the present numerical simulation for periodic fully developed flow under constant wall temperature for a corrugated duct with rounded corners. Representative results were carried out for a Prandtl number of 0.7 in the Reynolds number range from 100 to 1000 for three corrugation angles of 15°, 30°, 45° and for four aspect ratios.

GOVERNING EQUATIONS AND BOUNDARY CONDITIONS

The problem considered in this study is schematically shown in Fig. 1(a). As seen in this figure, the walls which form the duct are infinitely long in the y-direction. The geometry of the duct is specified by the cycle length (L), the width of the duct (H'), and the corrugation angle (θ) which is the slope of the duct boundaries at positions $y = L/4$ and $3L/4$. The deviation of the left wall from the y-axis $\delta(y)$ is expressed as

$$\delta(y) = [(L/4)\tan\theta][1-(2/\pi)\cos(2\pi y/L)]. \quad (1)$$

The dashed lines in Fig. 1(a) represent the duct boundaries with sharp corners. These boundaries coincide with the approximated cosine boundaries at the positions $y = L/4$ and $3L/4$.

The fluid flow attains a periodic fully developed condition sufficiently far from the inlet. The general concepts of this periodically fully developed flow and heat transfer are discussed in ref. [11]. In such flows, the velocity field repeats itself at corresponding axial stations in successive cycles. The pressure does not obey the same type of periodicity condition since it

NOMENCLATURE

A_w per-cycle heat transfer surface area
B dimensionless per-cycle pressure gradient, equation (8)
H' duct width
h, h_m local and average heat transfer coefficients, equation (21)
K thermal conductivity
L axial length of a cycle
$\dot{m}$ total mass flow rate
Nu, Nu_m local and average Nusselt numbers, equation (24)
P dimensionless periodic pressure, equation (8)
p, p' pressure and periodic pressure
Δp per-cycle pressure drop
Pr Prandtl number
q, Q local heat flux and per-cycle wall heat transfer rate
Re Reynolds number, equation (18)
T dimensionless temperature
t, t_b, t_w temperature, bulk temperature, and wall temperature
U, V dimensionless velocity components, $u/(\nu/L)$, $v/(\nu/L)$
X, Y dimensionless transverse and axial coordinates, x/L, y/L
x, y transverse and axial coordinates.

Greek symbols
β per-cycle pressure gradient
δ, Δ deviation of wall and its dimensionless form, $\delta(y)/L$
θ corrugation angle
λ bulk temperature gradient parameter, equation (14)
ρ density
σ right-hand side of equation (12)
Ψ, Ψ_w stream function $[= \int_0^{H'/L} V\,d\eta]$ and its value at the right wall.

Subscripts
)) corrugated duct with rounded corners
» corrugated duct with sharp corners
‖ straight duct.

decreases in the y-direction. Therefore, it is expressed as

$$p(x,y) = -\beta y + p'(x,y) \tag{2}$$

where β is a constant, defined as

$$\beta = [p(x,y) - p(x,y+L)]/L \tag{3}$$

and p' behaves in a periodic manner from module to module as

$$p'(x,y) = p'(x,y+L) = p'(x,y+2L) = \ldots \tag{4}$$

For the case of the uniform wall temperature boundary condition, the fluid temperature approaches the wall temperature in the fully developed region. A dimensionless temperature is defined as

$$T(x,y) = [t(x,y) - t_w]/(t_b - t_w) \tag{5}$$

where

$$t_b - t_w = \int (t - t_w) v\,dx \Big/ \int v\,dx. \tag{6}$$

For a periodically thermally developed region, the dimensionless temperature satisfies the following relationship:

$$T(x,y) = T(x,y+L) = T(x,y+2L) = \ldots \tag{7}$$

Therefore, the fully developed dimensionless temperature field repeats itself at corresponding axial stations in successive cycles.

The governing equations to be considered are the continuity, momentum, and energy equations. Constant thermophysical properties are assumed and natural convection is excluded. The following dimensionless variables are used:

$$X = x/L, \quad Y = y/L, \quad U = u/(\nu/L), \quad V = v/(\nu/L),$$
$$P = p'/\rho(\nu/L)^2, \quad B = \beta L/\rho(\nu/L)^2. \tag{8}$$

Then, upon the introduction of the dimensionless variables and parameters, the governing equations take the following forms:

$$\partial U/\partial X + \partial V/\partial Y = 0 \tag{9}$$

$$U\partial U/\partial X + V\partial U/\partial Y = \partial^2 U/\partial X^2 + \partial^2 U/\partial Y^2 - \partial P/\partial X \tag{10}$$

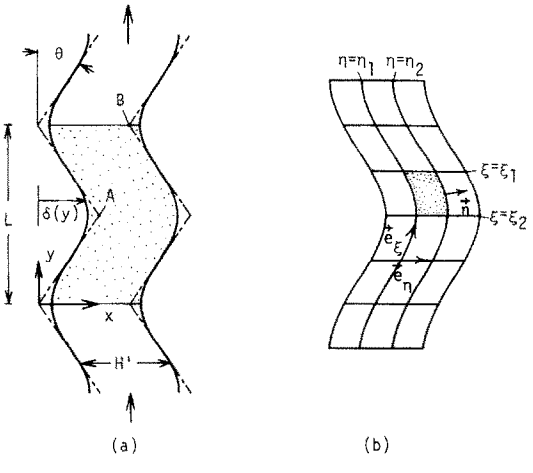

FIG. 1. (a) Schematic diagram of a corrugated duct. (b) Lines of constant η and ξ in the physical domain.

$$U\partial V/\partial X+V\partial V/\partial Y=\partial^2 V/\partial X^2+\partial^2 V/\partial Y^2-\partial P/\partial Y+B \quad (11)$$

$$U\partial T/\partial X+V\partial T/\partial Y=\partial^2 T/\partial X^2+\partial^2 T/\partial Y^2+\sigma/Pr \quad (12)$$

where

$$\sigma=[2(\partial T/\partial Y)-Pr\,VT]+T(\lambda^2+\partial\lambda/\partial Y) \quad (13)$$

and

$$\lambda=[\mathrm{d}(t_b-t_w)/\mathrm{d}Y](t_b-t_w). \quad (14)$$

The terms σ and λ are periodic parameters arising from the assumptions of the constant wall temperature boundary condition. These values are determined as part of the solution process.

To complete the formulation of the problem in the physical domain, the boundary conditions remain to be discussed. These are

$$\text{on the walls: } U=V=0, \quad T=0\ (t=t_w). \quad (15)$$

At the inlet and outlet ends of the solution domain, periodic conditions are imposed.

SOLUTION METHODOLOGY

The solution methodology based on the coordinate transformation is fully described by one of the authors [9] and is well documented in earlier papers [8, 12]. Specifically, the X, Y coordinates are transformed into η, ξ coordinates by the relationship

$$\eta=X-\Lambda(Y), \quad \xi=Y \quad (16)$$

where

$$\Delta(Y)=\delta(y)/L.$$

In terms of the new coordinates, the values of η on both wall boundaries take 0 and H'/L, respectively. Then, the solution domain is defined by $0<\eta<H'/L$, $0<\xi<1$. Lines of constant η and ξ are illustrated in Fig. 1(b). The transformed governing differential equations are integrated over the control volume contained between lines $\eta=\eta_1,\eta_2$ and $\xi=\xi_1,\xi_2$. The discretized procedure of the integrated equations is based on the power-law scheme of Patankar [13]. The pressure and velocities are linked by the SIMPLE algorithm of Patankar [13], and the discretized equations are solved by using a line-by-line method [14].

The numerical computations were performed for a Prandtl number of 0.7 and for $\theta=15°, 30°, 45°$. If the peaks of both the right and left walls with sharp edged corners lie in the same plane, the width H' is a function of θ and L as

$$H'=(L/2)\tan\theta. \quad (17)$$

Then the selected values of H'/L range from $(\tan\theta)/4$ to $\tan\theta$. Five values of the dimensionless pressure gradients B were selected in such a way that the calculated Reynolds numbers are 100, 200, 500, 700, and 1000.

The computations were performed with (18×34) grid points. These grid points were distributed in a non-uniform manner with higher concentration of grids close to the corrugated walls. Each interior control volume contains one grid point, while the boundary adjacent control volume contains two grid points. Supplementary runs were performed with (26×50) and (34×66) grid points to investigate the grid size effect for the case of $H'/L=0.1443$ and $\theta=30°$. Three values of the dimensionless pressure gradient B were selected in such a way that the calculated Reynolds numbers ranged from 100 to 1000. The results are listed in Table 1. The maximum change in the Reynolds and Nusselt numbers, respectively, between the coarse mesh (18×34) and the fine mesh (34×66) were within 2 and 7% at identical pressure gradients. Thus, the coarse mesh (18×34) was chosen to maintain relatively moderate computer costs.

Attention will now be directed to the calculation of the Reynolds number which will be defined as

$$Re=2\dot{m}/\mu \quad (18)$$

where the mass flow rate $\dot{m}$ is given by

$$\dot{m}=\mu\int_0^{H'/L} V_{Y=0}\,\mathrm{d}\eta. \quad (19)$$

Another quantity of interest is the calculation of the pressure drop for one cycle. It is of practical interest to compare this quantity with the corresponding value obtained for the straight duct (plane Poiseuille flow) with width H'. This ratio can be expressed as follows:

$$(\Delta p/L)_{))}/(\Delta P/L)_{\|}=[B/(6Re)](H'/L)^3. \quad (20)$$

Finally, the local heat transfer coefficient h and cycle average heat transfer coefficient h_m will be defined as

$$h=q/(t_w-t_b), \qquad h_m=Q/A_w\overline{(t_w-t_b)} \quad (21)$$

where q is the local heat flux, A_w is the per-cycle transfer surface area, Q is the heat transfer rate from both walls to the fluid per cycle, and $\overline{t_w-t_b}$ is the average bulk-to-wall temperature difference. The log–mean temperature difference is expressed as

$$\overline{t_w-t_b}=(t_w-t_b)_{Y=0}(1-\gamma)\Big/\left(-\int_0^1\lambda\,\mathrm{d}Y\right) \quad (22)$$

where

$$\gamma=\exp\int_0^1\lambda\,\mathrm{d}Y. \quad (23)$$

The Nusselt number expressions were obtained by assuming a log–mean temperature difference as follows:

Table 1. Grid size effect on Reynolds number and average Nusselt number

	18 × 34		26 × 50		34 × 66	
B	Re	Nu_m	Re	Nu_m	Re	Nu_m
360 000	129.3	7.994	128.0	8.041	127.5	8.057
800 000	272.2	8.079	269.9	8.087	269.0	8.083
4 500 000	1062	10.03	1049	9.593	1041	9.298

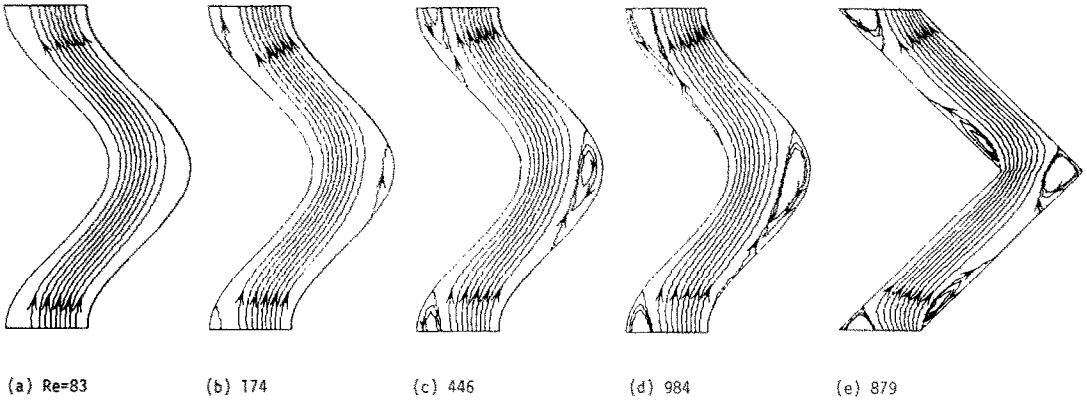

FIG. 2. Streamline diagram for $H'/L = 0.25$ with $\theta = 45°$ and Re as parameters.

$$Nu = h(2H')/K$$
$$= [1+(\partial\Delta/\partial Y)^2]^{0.5}(2H'/L)(\partial T/\partial\eta)$$
$$Nu_m = h_m(2H')/K$$
$$= -(2L/A_w)\int_0^1 \lambda\, dY(H'/L)\left[(Re\,Pr/2)\right.$$
$$\left. -\int_0^{H'/L}(\lambda T+\partial T/\partial Y)_{Y=0}\, d\eta\right]. \quad (24)$$

RESULTS AND DISCUSSION

The streamline maps obtained from the solutions are presented in Fig. 2. These figures are for $H'/L = 0.25$ and $\theta = 45°$, and in the Reynolds number range from about 80 to 1000. Results for the sharp cornered duct are also presented in Fig. 2(e). The contour interval $\Delta\Psi/\Psi_w$ is chosen as 0.1 for the core flow. The values of the contour line Ψ/Ψ_w on the left and on the right walls are 0 and 1, respectively. The contour interval $\Delta\Psi/\Psi_w$ in the separation bubble is 0.01. No separation bubble can be seen at low Reynolds number $Re < 150$ (Fig. 2(a)). For $Re > 150$, a separation bubble can be seen at the valley of the corner. As expected, the separation bubble increases in length with Reynolds number because the fluid is unable to turn sharply to follow the wall at higher Reynolds number (Fig. 2(d)). Although one separation bubble can be seen for the round cornered duct, two separation bubbles can be seen at the valley of the sharp cornered duct (Fig. 2(e)).

Representative results for the pressure drop ratios are plotted as a function of Reynolds number in Fig. 3 with H'/L and θ as curve parameters. These ratios are determined numerically by dividing Δp of the corrugated duct into the corresponding values of the straight duct (plane Poiseuille flow) with an equal width H'. For this case, the mass flow rate in the corrugated duct and in the straight duct is the same. The dashed lines in Fig. 3 indicate the results for the sharp cornered duct. The pressure drop ratios for both the sharp and round cornered ducts are greater than

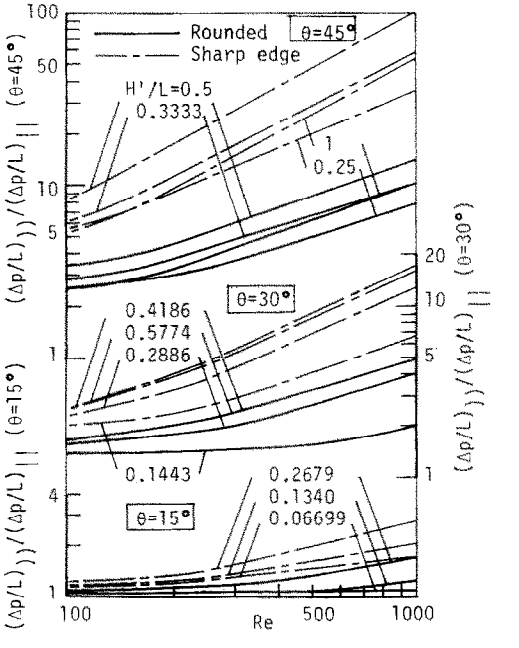

FIG. 3. Comparison of pressure drops for corrugated and straight ducts.

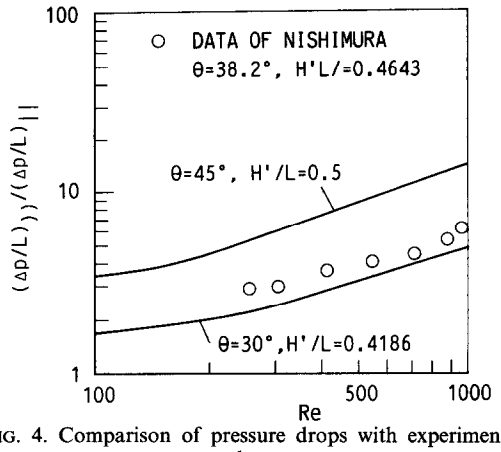

FIG. 4. Comparison of pressure drops with experimental data.

one, as expected. The pressure drop for the round cornered duct is less than that of the sharp cornered duct. It is noteworthy that the pressure drop for the round cornered duct of $\theta = 45°$ is 80% (maximum) less than that of the sharp cornered duct at $Re = 1000$.

The experimental data of Nishimura *et al.* [15] are compared with the present computation in Fig. 4. The experimental data are for a duct with $H'/L = 0.4643$ and $\theta = 38.2°$ and the computational results are for ducts of $H'/L = 0.5$, $\theta = 45°$ and for $H'/L = 0.4186$, $\theta = 30°$. Even though direct comparison of the experimental and numerical results are not possible but the present computation is consistent with the experiment.

Representative results for the local Nusselt number are presented in Figs. 5(a)–(c) for the duct geometry represented by $H'/L = 0.25$ and $\theta = 45°$. The result for the sharp cornered duct is also presented in Fig. 5(d). The local Nusselt number for the round cornered duct takes high values from the reattachment point through the peak of the corner, and it takes low values on the rear facing facet, while the local Nusselt number for the sharp cornered duct takes high values at the reattachment point and decreases from the reattachment point through the peak of the corner and changes abruptly at the peak of the corner (Fig. 5(d)). The local Nusselt number distribution in the y-direction is very sensitive to the rounding of the corners.

Results for the periodic fully developed Nusselt number as a function of the Reynolds number are plotted in Fig. 6 with H'/L and θ as curve parameters. The Nusselt number is determined using equation (24) where the log–mean temperature difference is used. It should be noted that the value for the Nusselt number for the fully developed straight duct is 7.54 and is independent of both the Reynolds and Prandtl numbers. However, it is evident from the governing equations that the periodic fully developed Nusselt number is a function of the Reynolds number, Prandtl number, geometric parameters H'/L and θ. The periodic fully developed Nusselt numbers are greater than 7.54 depending on the parameters. The results for the sharp cornered duct are also presented in Fig. 6. The Nusselt number for the round cornered duct is 40% lower than that for the sharp cornered duct ($\theta = 45°$) at high Reynolds number.

In appraising the performance of the round cornered duct configuration relative to the corresponding value for a straight duct with interwall spacing (measured perpendicular to the walls) H', comparisons will be made for three different constraints [16]: (1) identical pumping power PP, (2) identical pressure drop per-cycle $\Delta p/L$, and (3) identical mass flow rate $\dot{m}$. The heat transfer rate from the walls to the fluid per-cycle, Q, is obtained by equations (21)–(24) as follows:

$$Q = (Nu_m K/2H')(t_w - t_b)_{Y=0} \times (1-\gamma)A_w \Big/ \left(-\int_0^1 \lambda \, dY\right). \quad (25)$$

The heat transfer rate ratios for three different con-

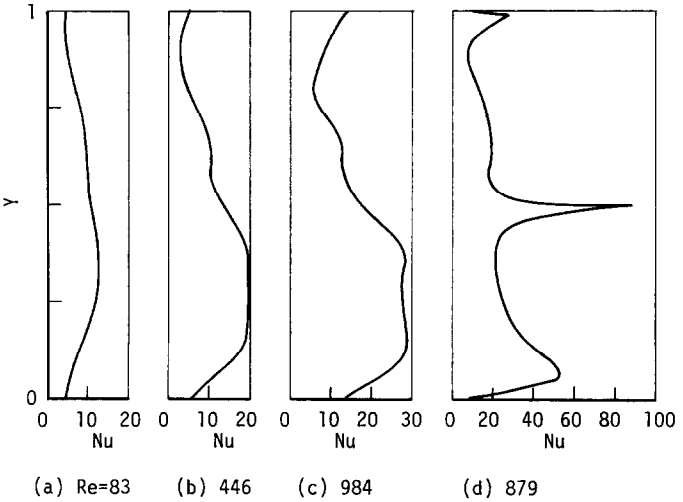

FIG. 5. Local Nusselt numbers for $H'/L = 0.25$ with $\theta = 45°$ and Re as parameters.

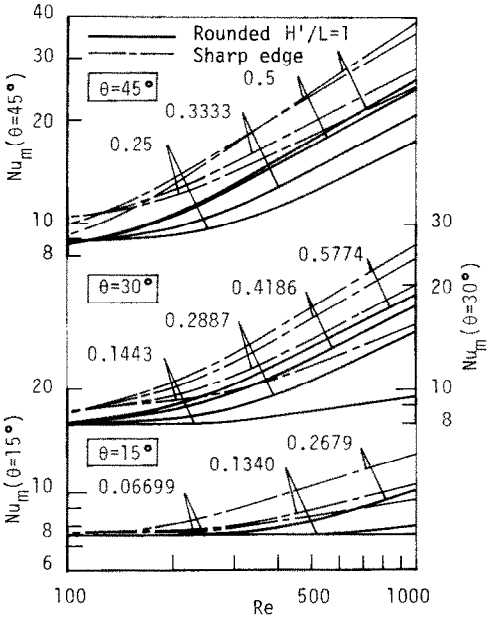

FIG. 6. Average Nusselt numbers for a corrugated duct as a function of Re.

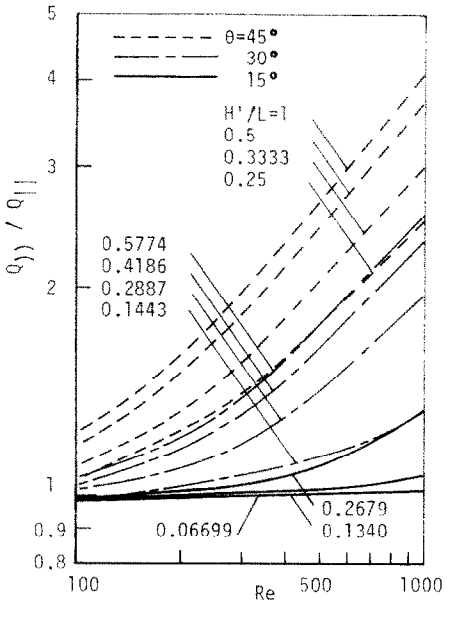

FIG. 7. Heat transfer rate ratios $Q_{))}/Q_{\|}$ as a function of $Re_{))}$ for identical pumping power.

straints are plotted as a function of Reynolds number in Figs. 7–9 with H'/L and θ as curve parameters. These ratios are determined numerically by dividing Q for the round cornered duct into corresponding values of the straight duct. The results for identical pumping power, identical pressure drop per-cycle, and identical mass flow rate are shown in Figs. 7–9, respectively. As seen in the figures, the heat transfer rate ratios are greater than one at higher Reynolds number for all cases. The pumping power is equal to the product of the pressure drop and the volume flow given by $PP \approx m(\Delta p/L)$. In the case of identical pumping power, the following relation between the pumping power of the round cornered duct and the straight duct is given

$$\dot{m}\beta_{))} = \dot{m}\beta_{\|}. \tag{26}$$

In dimensionless form, it is expressed by

$$Re_{))}\, B_{))} = Re_{\|}\, B_{\|}. \tag{27}$$

The following relationship between Reynolds number and dimensionless pressure gradient parameter B of the straight duct is also given:

$$Re_{\|} = B_{\|}(H'/L)^3/6. \tag{28}$$

Substituting equation (28) into equation (27), the Reynolds number for the straight duct can be obtained for a pumping power equal to that of the round cornered duct as

$$Re_{\|} = [(H'/L)^3\, Re_{))}\, B_{))}/6]^{1/2}. \tag{29}$$

In the case of identical pressure drop per-cycle, the Reynolds number of the straight duct can be expressed by

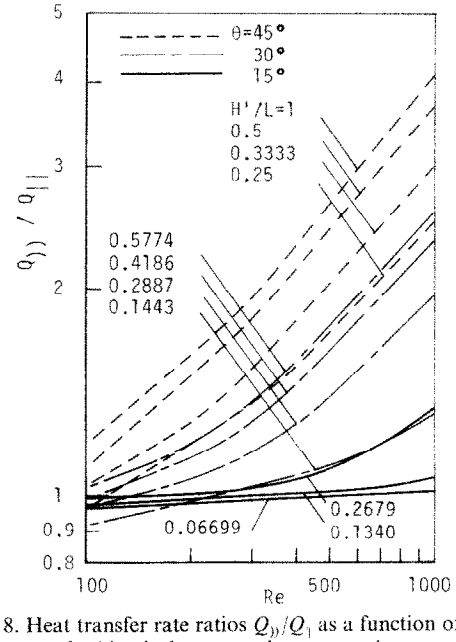

FIG. 8. Heat transfer rate ratios $Q_{))}/Q_{\|}$ as a function of $Re_{))}$ for identical pressure drop per cycle.

$$Re_{\|} = B_{))}(H'/L)^3/6. \tag{30}$$

In the case of identical mass flow rate, the Reynolds number of the straight duct can be expressed by

$$Re_{\|} = Re_{))}. \tag{31}$$

The heat transfer rate ratios for three different constraints are plotted as a function of Reynolds number in Figs. 10–12 with H'/L and θ as curve parameters. These ratios are determined numerically by dividing Q for a round cornered duct into the corresponding values of the sharp cornered duct. The subscript »

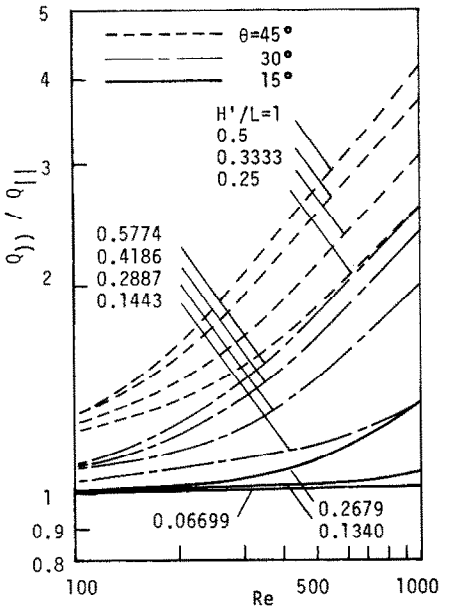

FIG. 9. Heat transfer rate ratios $Q_{))}/Q_{\|}$ as a function of $Re_{))}$ for identical mass flow.

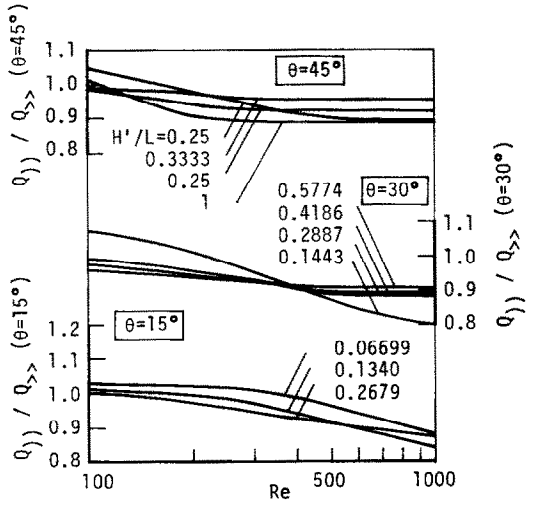

FIG. 10. Heat transfer rate ratios $Q_{))}/Q_{\gg}$ as a function of $Re_{))}$ for identical pumping power.

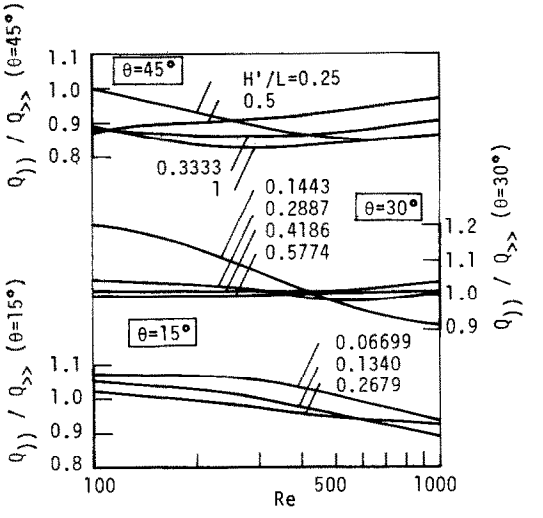

FIG. 11. Heat transfer rate ratios $Q_{))}/Q_{\gg}$ as a function of $Re_{))}$ for identical pressure drop per cycle.

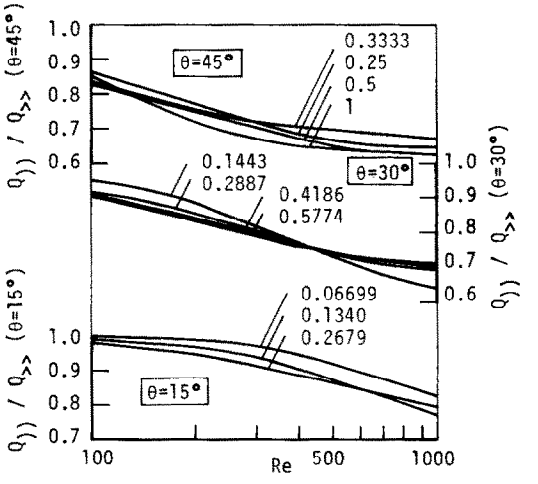

FIG. 12. Heat transfer rate ratios $Q_{))}/Q_{\gg}$ as a function of $Re_{))}$ for identical mass flow.

refers to the corrugated duct with sharp corners. The results for identical pumping power, identical pressure drop per-cycle, and identical mass flow rate are shown in Figs. 10–12, respectively. As seen in these figures, the heat transfer rate ratios are greater than or less than one, depending on the value of H'/L and θ and also the specific constraints under consideration. The heat transfer rate for the round cornered duct is 20 and 35% (maximum) less than that for the sharp cornered duct under identical pumping power and identical mass flow rate, respectively, while it is 20% (maximum) greater than that for the sharp cornered duct under identical pressure drop per-cycle.

CONCLUDING REMARKS

Periodic, fully developed heat transfer and fluid flow characteristics of the corrugated duct with rounded corners using a cosine function approximation were obtained by a finite difference technique and utilization of a coordinate transformation methodology. The main conclusions of the results are given below.

(a) The pressure drop per-cycle for the corrugated ducts for both sharp corners and round corners are greater than that for the straight duct. The pressure drop for the round cornered duct is 80% (maximum) less than that for the sharp cornered duct.

(b) The heat transfer rate for the round cornered duct is greater than that for the straight duct under identical pumping power and identical mass flow, while it is greater than or less than that for the straight duct under identical pressure drop. At higher

Reynolds number, the heat transfer rate for the round cornered duct is greater than that for the straight duct under all constraints.

(c) The heat transfer rate for the round cornered duct is greater than or less than that for the sharp cornered duct, depending on duct geometry and on the constraints. The heat transfer rate for the round cornered duct is 20 and 35% (maximum) less than that for the sharp cornered duct under identical pumping power and identical mass flow, respectively, while it is 20% (maximum) greater than that for the sharp cornered duct under identical pressure drop per cycle.

REFERENCES

1. R. Izumi, H. Yamashita and K. Oyakawa, Fluid flow and heat transfer in corrugated wall channels (1st Report, Analysis in the case where channels are bent perpendicularly two times), *Bull. J.S.M.E.* **24**(194), 1425–1432 (1981).
2. R. Izumi *et al.*, Fluid flow and heat transfer in corrugated wall channels (3rd Report, Effects of bending angles in the case where channels are bent two times), *Bull. J.S.M.E.* **26**(216), 1027–1035 (1983).
3. R. S. Amano, Laminar heat transfer in a channel with two right-angled bends, *J. Heat Transfer* **106**, 591–596 (1984).
4. R. S. Amano, Turbulent heat transfer in a channel with two right-angled bends, AIAA Paper No. 84-04094, AIAA Aerospace Sciences Meeting, Reno, January (1984).
5. R. Izumi *et al.*, Fluid flow and heat transfer in corrugated wall channels (2nd Report, Experiments in the case where channels are bent perpendicularly two times), *Bull. J.S.M.E.* **24**(198), 2098–2106 (1981).
6. R. Izumi, H. Yamashita and K. Oyakawa, Fluid flow and heat transfer in corrugated wall channels (4th Report, Analysis in the case where channels are bent many times), *Bull. J.S.M.E.* **26**(217), 1146–1153 (1983).
7. R. S. Amano, A numerical study of laminar and turbulent heat transfer in a periodically corrugated wall channel, *J. Heat Transfer* **107**, 564–569 (1985).
8. Y. Asako and M. Faghri, Finite-volume solutions for laminar flow and heat transfer in a corrugated duct, *J. Heat Transfer* **109**, 627–634 (1987).
9. M. Faghri, E. M. Sparrow and A. T. Prata, Finite difference solutions of convection-diffusion problem in irregular domains using a non-orthogonal coordinate transformation, *Numer. Heat Transfer* **7**(2), 183–209 (1984).
10. E. M. Sparrow and L. M. Hossfeld, Effect of rounding of protruding edges on heat transfer and pressure drop in a duct, *Int. J. Heat Mass Transfer* **27**, 1715–1723 (1984).
11. S. V. Patankar, C. H. Liu and E. M. Sparrow, Fully developed flow and heat transfer in ducts having streamwise-periodic variation of cross-sectional area, *J. Heat Transfer* **99**, 180–186 (1977).
12. M. Faghri and Y. Asako, Numerical determination of heat transfer and pressure drop characteristics for converging-diverging flow channel, *J. Heat Transfer* **109**, 606–612 (1987).
13. S. V. Patankar, A calculation procedure for two-dimensional elliptic situations, *Numer. Heat Transfer* **4**, 409–425 (1981).
14. S. V. Patankar, *Numerical Heat Transfer and Fluid Flow*, McGraw-Hill, New York (1980).
15. T. Nishimura, Y. Kajimoto and Y. Kawamura, Mass transfer enhancement in channels with wavy wall, *J. Chem. Engng Japan* **19**(2), 142–144 (1986).
16. E. M. Sparrow and J. W. Comb, Effect of interwall spacing and fluid flow inlet conditions on a corrugated-wall heat exchanger, *Int. J. Heat Mass Transfer* **26**, 993–1005 (1983).

TRANSFERT THERMIQUE ET PERTE DE CHARGE DANS UN TUBE CORRUGUE AVEC DES COINS ARRONDIS

Résumé—On détermine numériquement les caractéristiques de transfert de chaleur et de perte de charge pour un tube corrugué avec des coins arrondis. Les frontières sont approchées par des fonctions cosinus. Les calculs concernent un nombre de Prandtl de 0,7 et un domaine de nombre de Reynolds allant de 100 à 1000, pour trois angles de corrugation et pour quatre valeurs du rapport de forme. L'arrondissement des coins provoque une diminution du facteur de frottement et du nombre de Nusselt. La performance de transfert thermique du canal avec des angles arrondis est comparée à un canal rectiligne et à un canal avec des coins vifs, pour trois contraintes différentes: puissance de pompage donnée, perte de charge donnée, débit-masse fixé. Les transferts diminuent ou augmentent suivant les conditions spécifiques.

CHARAKTERISTIK DES WÄRMEÜBERGANGS UND DES DRUCKABFALLS IN EINEM WELLROHR MIT ABGERUNDETEN ECKEN

Zusammenfassung—Wärmeübergang und Druckabfall in einem Wellrohr mit abgerundeten Kanten wurden numerisch untersucht. Das Rohrprofil wurde mit einer Cosinus-Funktion angenähert. Für eine Prandtl-Zahl von 0,7 wurden Berechnungen im Reynolds-Zahl-Bereich von 100 bis 1000 ausgeführt, wobei jeweils drei verschiedene Wellungswinkel und vier geometrische Abmessungsverhältnisse berücksichtigt wurden. Eine Abrundung der Kanten hatte eine Verminderung des Reibungskoeffizienten und der Nusselt-Zahl zur Folge. Der Wärmeübergang in einem Rohr mit abgerundeten Kanten wurde mit dem eines geraden Rohrs und dem eines Rohrs mit scharfen Kanten unter drei verschiedenen Randbedingungen verglichen: konstante Pumpenleistung, konstanter Druckabfall und konstanter Massenstrom. Abhängig von den verschiedenen Bedingungen verringerte bzw. vergrößerte sich der Wärmeübergang.

ХАРАКТЕРИСТИКИ ТЕПЛОПЕРЕНОСА И ПЕРЕПАДА ДАВЛЕНИЯ В КАНАЛЕ С ГОФРИРОВАННЫМИ СТЕНКАМИ И СКРУГЛЕННЫМИ УГЛАМИ

Аннотация—Численно определяются теплообмен и перепад давления в канале с гофрированными стенками и скругленными углами. Границы канала аппроксимируются косинусом. Расчеты проводятся для числа Прандтля 0,7 в диапазоне значений числа Рейнольдса от 100 до 1000 для трех заданных значений угла рифления и четырех значений отношений сторон. Скругление углов приводит к уменьшению коэффициента трения и числа Нуссельта. Теплообмен в канале со скругленными углами сравнивается с теплообменом в прямом канале, имеющем острые углы, при следующих условиях: постоянные мощность прокачки, перепад давления и расход. Интенсивность теплообмена уменьшается или увеличивается в зависимости от условий.